First-principles study of oxygen-deficient LaNiO_{3} structures

Andrei Malashevich and Sohrab Ismail-Beigi

First-principles study of oxygen-deficient LaNiO$_3$ structures

Andrei Malashevich[1,2,*] and Sohrab Ismail-Beigi[1,2,3,4]

[1]*Center for Research on Interface Structures and Phenomena (CRISP),*
Yale University, New Haven, Connecticut 06520, USA
[2]*Department of Applied Physics, Yale University, New Haven, Connecticut 06520, USA*
[3]*Department of Physics, Yale University, New Haven, Connecticut 06520, USA*
[4]*Department of Mechanical Engineering and Materials Science,*
Yale University, New Haven, Connecticut 06520, USA

We describe the results of first-principles calculations of the properties of oxygen vacancies in LaNiO$_3$. We consider isolated oxygen vacancies, pairs of vacancies, and vacancies at finite concentrations that form oxygen-deficient phases of LaNiO$_3$. The key electronic structure question we address is whether and to what extent an oxygen vacancy acts as an electron donor to the Fermi level (mobile and conducting electronic states). More generally, we describe how one can quantify, based on electronic structure calculations, the extent to which a localized point defect in a metallic system donates electrons to the Fermi level compared to trapping electrons in localized defect states. For LaNiO$_3$, we find that an oxygen vacancy does not create mobile carrier but instead makes the two Ni sites adjacent to it turn into Ni^{2+} cations. Energetically, we compute the formation energy and diffusion barrier for oxygen vacancies. Structurally, we show that pair of vacancies prefer to form on opposite sides of a Ni cation, aligning along a pseudocubic axis. For finite concentrations of vacancies, we compute the dependence of the LaNiO$_3$ lattice parameters on the vacancy concentration to provide reliable data for experimental determination of oxygen content in LaNiO$_3$ and LaNiO$_3$ thin films.

I. INTRODUCTION

Rare-earth nickelate perovskite oxides, with chemical formula RNiO$_3$ were R is a rare-earth atom, continue to generate much scientific interest. The combined effect of the crystal structure and the electronic correlations of Ni d electrons in RNiO$_3$ systems results in a variety of interesting phenomena.[1–3] These phenomena include metal-insulator transitions (MITs),[4,5] spin-density waves,[5] charge order,[6–9] and complex magnetic structure at interfaces.[10] Among rare-earth nickelates, LaNiO$_3$ is the only one that remains metallic in bulk form down to the lowest measured temperatures. For this reason, LaNiO$_3$ is widely used as an electrode in oxide electronic devices, in particular in epitaxially strained perovskite thin films.[11–15] In addition, ultrathin films of LaNiO$_3$ were found to display thickness-dependent MITs.[16–18] Finally, much attention has been paid recently to layered heterostructures involving LaNiO$_3$ in a variety of attempts to engineer the electronic structure that would allow for high-temperature superconductivity.[16,17,19–31]

Many of the physical properties of metal oxides are sensitive to the presence of oxygen vacancies. In stoichiometric bulk LaNiO$_3$, Ni ion assumes 3+ charge state, while oxygen deficiency can result in the creation of Ni^{2+} ions, significantly affecting conductivity and MIT.[32–36] Sánchez et al.[32] examined bulk LaNiO$_3$, LaNiO$_{2.75}$, and LaNiO$_{2.5}$ and found that conductivity decreases as oxygen vacancy concentration δ increases and MIT occurs for $\delta \geq 0.25$. The observed behavior was explained based on a model positing that LaNiO$_3$ is a charge-transfer metal,[4,37] whereby the interplay between the bandwidths and energy gaps of the O $2p$ and Ni $3d$ bands determines conductivity. Later, more systematic studies of the dependence of electronic conduction in LaNiO$_{3-\delta}$ on δ were performed by several groups.[33,34] Gayathri et al.[33] also measured the Hall coefficient of a LaNiO$_3$ film and found it to be positive, meaning that the dominant charge carriers contributing to transport in LaNiO$_3$ are holes. Abbate et al.[35] studied the electronic structure of LaNiO$_{3-\delta}$ systems using x-ray absorption spectroscopy (XAS), a sensitive probe of the covalent mixing between the O $2p$ and transition metal $3d$ levels. They confirmed that charge carriers in bulk LaNiO$_3$ contain considerable oxygen character, and they related the MIT to the disappearance of charge carriers. Horiba et al.[38] performed x-ray photoemission spectroscopy (XPS) and XAS of LaNiO$_{3-\delta}$ thin films and found that the density of states near the Fermi level in these films is very sensitive to oxygen content. They also performed first-principles calculations of bulk LaNiO$_3$ under strain and found that strain alone cannot explain the experimentally observed narrowing of the Ni $3d$ e_g peak at the Fermi level. Using XPS deconvolution analysis, Qiao and Bi[39] were able to distinguish Ni^{3+} and Ni^{2+} formal valence states in LaNiO$_{3-\delta}$ films which allowed them to determine oxygen stoichiometry δ accurately. As expected from previous studies, they found that with decrease of the Ni^{3+}/Ni^{2+} ratio, the LaNiO$_{3-\delta}$ films turn semiconducting. These authors also performed first-principles calculations for several LaNiO$_{3-\delta}$ structures and showed that at sufficiently large δ band gap appears due to narrowing of valence and conduction bands.

Despite the significant progress in the understanding of electronic structure of LaNiO$_{3-\delta}$ systems on the experi-

mental side, there was less work done on the theory side, including first-principles calculations. In this work, we provide a first-principles survey of the basic properties of oxygen vacancies in $LaNiO_3$. The questions we address are: (i) Do oxygen vacancies act as electron donors to mobile conducting states at the Fermi level in $LaNiO_3$? (ii) Generally, how does one use electronic structure calculations to decide to what extent a point defect donates mobile carriers compared to trapping them in defects states? (iii) How difficult is it to form an oxygen vacancy in $LaNiO_3$? How mobile is it once formed? For example, do we expect vacancies to be sufficiently mobile to readily diffuse in the crystal and achieve the equilibrium structure at the level of oxygen deficiency? (iv) What is the nature of the interaction between oxygen vacancies: do they repel or attract and prefer to form complexes? (v) What is the theoretically expected effect of the finite oxygen vacancy concentration on the lattice parameters of oxygen deficient $LaNiO_{3-\delta}$ systems?

The paper is organized as follows. Section II describes the technical details of our numerical calculations. In Sec. III, our main results are presented, followed by the summary and conclusions in Sec. IV.

II. COMPUTATIONAL METHODS

In this work, we are primarily interested in the ground state properties of oxygen-reduced $LaNiO_3$ systems, based on the calculations of total energies, ground-state electron densities, and crystal structures. For this reason, we use density-functional theory (DFT) for our calculations. DFT can already describe many of the physical properties of bulk $LaNiO_3$[40] or $LaNiO_3$ thin films[18], and we expect this to carry over to the basic properties of oxygen vacancies. Proper treatment of charged defects in general may require many-body corrections for calculations of defect formation energies as demonstrated explicitly in certain insulating systems.[41,42] However, in our case $LaNiO_3$ is robustly metallic, so that defects are well screened and should be neutral and such many-body effects should be of less importance.

We performed first-principles calculations in a plane-wave pseudopotential basis. The calculations were done with the QUANTUM ESPRESSO software package.[43] We chose local-density approximation (LDA) for the exchange-correlation functional since it was shown previously by Gou *et al.*[40] that LDA adequately reproduces the crystal and electronic structure of bulk $LaNiO_3$ and in fact may be the best choice among available exchange-correlation functionals. The LDA exchange-correlation potential was parameterized using the Perdew-Zunger method.[44] For the computation of the formation energy of oxygen vacancies, we also cross-checked our results by using the PBE generalized gradient approximation as well.[45] In this work, we report on non-magnetic LDA calculations and not spin-polarized LSDA: bulk $LaNiO_3$ is a paramagnetic metal. Furthermore, we have explicitly

TABLE I. Pseudopotential reference valence configurations and corresponding cutoff radii (atomic units).

Atom	Valence configuration	r_c^s	r_c^p	r_c^d
La	$5s^2 5p^6 5d^1 6s^{1.5} 6p^{0.5}$	2.2	2.0	2.2
Ni	$3d^8 4s^2 4p^0$	2.0	2.0	2.2
O	$2s^2 2p^6$	1.3	1.3	$\cdots$

performed spin-polarized LSDA calculations that show that an isolated neutral oxygen vacancy ($2 \times 2 \times 2$ supercell) does not develop magnetization.

The electron-ion interactions were described by Vanderbilt ultrasoft pseudopotentials.[46] The pseudopotentials were generated with the USPP-7.3.6 package[47] with parameters listed in Table I. For lanthanum and nickel, nonlinear core corrections were applied.[48] The La 4f states were not explicitly generated or described: La assumes 3+ valence state in $LaNiO_3$ with the empty 4f shell so that these states should not be critical in terms of bonding. *A posteriori*, calculations that do not use La 4f states show excellent agreement with experiment.[18,31,40] The kinetic energy cutoff for the plane waves was set to $35\,Ry$ and the corresponding energy cutoff for the charge density was set to $280\,Ry$. For the primitive unit cell of bulk $LaNiO_3$ (described in detail below), the corresponding Brillouin zone was sampled by a uniform $12 \times 12 \times 12$ grid of k points. Equivalent meshes of k points were used for the larger supercells. The Brillouin zone integrations were done using the Gaussian smearing method with the smearing width of 1 mRy. The structural relaxations were performed until the Cartesian components of forces on all atoms were less than 3 meV/Å and stress tensor components were less than 0.1 kbar.

For the bulk and the $2 \times 2 \times 2$ supercells, we constructed maximally localized Wannier functions[49,50] (MLWFs) for analysis of the electronic structure. For this purpose, we used $9 \times 9 \times 9$ and $5 \times 5 \times 5$ grids of k points, respectively for the primitive 10-atom bulk unit cell and $2 \times 2 \times 2$ supercell. The Wannier functions were generated using the Wannier90 software package.[51] The Wannier functions correspond to a pd model for the system: 3 Wannier functions of p symmetry are obtained for each oxygen site and 5 Wannier functions of d symmetry for each nickel site. In $LaNiO_3$, the oxygen 2p and Ni 3d valence and conduction bands, taken together as a complex, are separated from all other bands by energy gaps. Hence, the choice of energy window for MLWFs generation was straightforward: to include these bands alone.

III. RESULTS

A. Bulk $LaNiO_3$

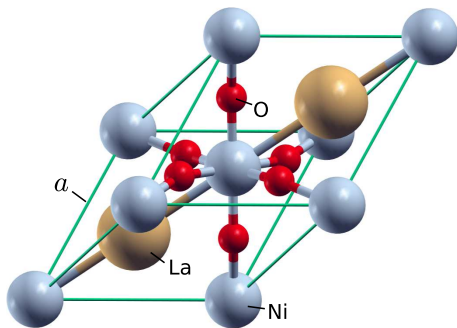The ground state of bulk $LaNiO_3$ assumes a rhombohedrally distorted perovskite structure. The symmetry

FIG. 1. (Color online) Primitive cell of LaNiO$_3$.

TABLE II. Structural parameters of bulk LaNiO$_3$ (R$\bar{3}$c space group) in the rhombohedral setting.

	Present work	Previous theory[a]	Experiment[b]
a (Å)	5.25	5.32	5.38
α (°)	61.4	61.4	60.9
x	0.809	0.801	0.797

[a] LDA results using QUANTUM ESPRESSO from Ref. 40.
[b] Ref. 5.

of this structure is given by the R$\bar{3}$c space group. The primitive unit cell has two formula units (10 atoms) and is shown in Fig. 1. In the rhombohedral setting, the unit cell can be described by the length of the lattice vectors, a, and the angle α between any two lattice vectors. The La, Ni, and O atoms occupy the $2a(\frac{1}{4}, \frac{1}{4}, \frac{1}{4})$, $2b(0, 0, 0)$, and $6e(x, \frac{1}{2} - x, \frac{1}{4})$ Wyckoff positions, respectively. Our calculated structural parameters for bulk LaNiO$_3$ are shown in Table II. The table also reproduces previous theoretical and experimental structural parameters indicating very satisfactory agreement.

The computed electronic band structure of the bulk is shown in Fig. 2. We also projected the bands shown in the figure onto Wannier functions with Ni $3d$ and O $2p$ characters. We note two important facts from the figure. First, the top of the O $2p$ dominated valence bands is 1 eV below the Fermi level: this means we can assign the formal charge state O^{2-} to the oxygen atoms in the bulk. Second, the Fermi level cuts through the conduction bands which have Ni $3d$ character so we have the formal charge state Ni^{3+} for nickel atoms in the bulk. These basic facts are important when understanding the electronic behavior of oxygen vacancies.

B. Isolated oxygen vacancy

In order to simulate an isolated neutral oxygen vacancy, we began by constructing a supercell of bulk LaNiO$_3$ corresponding to a $2 \times 2 \times 2$ pseudocubic perovskite structure with 40 atoms in the supercell. The explicit relation between the 40-atom pseudocubic $2 \times 2 \times 2$ cell and the primitive 10-atom cell shown in Fig. 1 is the
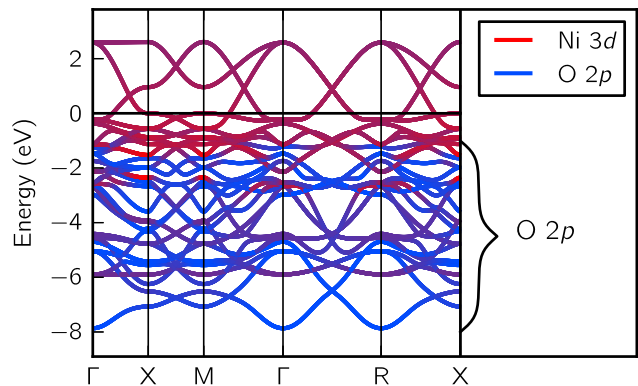

FIG. 2. (Color online) Calculated electronic band structure of bulk LaNiO$_3$ in the 10 atom unit cell projected on the Ni $3d$ (red) and O $2p$ (blue) Wannier functions. The high-symmetry points of the Brillouin zone are labeled using the convention for a corresponding simple perovskite cubic 5-atom unit cell; i.e., the axial directions connect neighboring Ni cations.
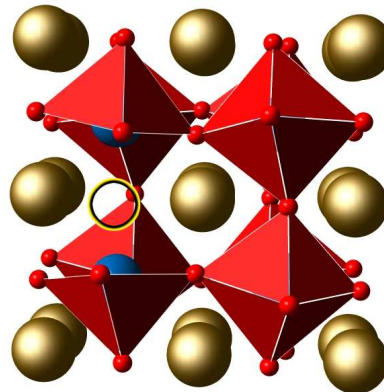

FIG. 3. (Color online) The $2 \times 2 \times 2$ pseudocubic supercell of LaNiO$_3$ with a single oxygen vacancy showing NiO$_6$ octahedra. The position of the vacancy is indicated by the black circle.

following. Let $\mathbf{a_1} = a(0, 1, 1)/\sqrt{2}$, $\mathbf{a_2} = a(1, 0, 1)/\sqrt{2}$ and $\mathbf{a_3} = a(1, 1, 0)/\sqrt{2}$ be the lattice vectors for the 10-atom cell. The the lattice vectors of the 40-atom cell are $\sqrt{2}(-\mathbf{a_1} + \mathbf{a_2} + \mathbf{a_3})$, $\sqrt{2}(\mathbf{a_1} - \mathbf{a_2} + \mathbf{a_3})$ and $\sqrt{2}(\mathbf{a_1} + \mathbf{a_2} - \mathbf{a_3})$.

We then removed one neutral oxygen atom as indicated in Fig. 3 which was chosen to be an O bonded along the unit cell z direction between its two Ni neighbors (we note that all O atoms are identical in this unit cell so this is simply a convenient choice for analysis).

Since the formal charge state of oxygen is O^{2-} in the bulk, it is expected that the removal of a neutral oxygen atom will liberate two electrons which will then redistribute in the defective system. This process is expected regardless of the fact that there is significant covalency in LaNiO$_3$[52]: since the oxygen $2p$ valence bands are well below the Fermi level, creating the neutral vacancy will add two electrons to the system. The main question is
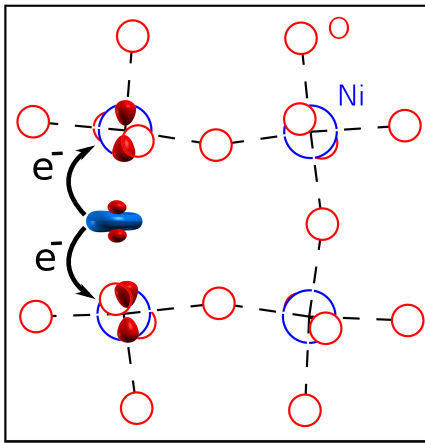
FIG. 4. (Color online) Theoretically calculated 3D electron redistribution function $\rho(V_O)+\rho(O)-\rho(\text{bulk})$ in LaNiO$_3$ upon neutral oxygen vacancy formation. Red (blue) 3D isosurfaces shows the increase (decrease) of the electron density in space. Arrows indicate the primary direction of electron redistribution from the vacancy site to the $d_{3z^2-r^2}$ orbitals of the two Ni neighboring the vacancy. The isosurfaces are drawn at $\sim 20\%$ of the maximum value of the electron density. The smaller red (larger blue) circles denote the O (Ni) atoms. The black dashed lines indicate the Ni–O bonds. The electron redistribution is highly localized.

where the two electrons end up going. There are three basic possibilities: (i) both electrons delocalize and are mobile so they raise the Fermi level and lead to n-type doping of LaNiO$_3$; (ii) both become bound to and localized around the vacancy site and thus do not dope the system; or (iii) some intermediate situation is reached where some part are bound and some part are mobile. As we explain below, our calculations conclude that scenario (ii) is correct.

We begin in real space where we compute the electron density redistribution. We compute the electron densities of the fully relaxed system with a vacancy $\rho(V_O)$, of a bulk-like LaNiO$_3$ $\rho(\text{bulk})$ where the oxygen atom is added back (with no structural relaxation), and of a neutral oxygen atom at the vacancy position in the otherwise empty supercell $\rho(O)$ (see Fig. 3). The redistribution $\Delta\rho = \rho(V_O) + \rho(O) - \rho(\text{bulk})$ is plotted in Fig. 4. We clearly see that oxygen vacancy donates electron charge to the $d_{3z^2-r^2}$ orbitals of the nearest two Ni atoms (where local z axes are directed from the two neighboring Ni sites towards the vacancy). Furthermore, the electron redistribution appears to be extremely localized in space and confined to the two Ni neighbors only. While an O vacancy *formally* donates two electrons to the system, and it appears that one electron goes to each neighboring Ni, actual values of electron transfer depend strongly on the method used to do the counting. A Löwdin analysis of orbital populations shows that only 0.1 electrons is transferred to $d_{3z^2-r^2}$ orbitals of each of the two nickel atoms.
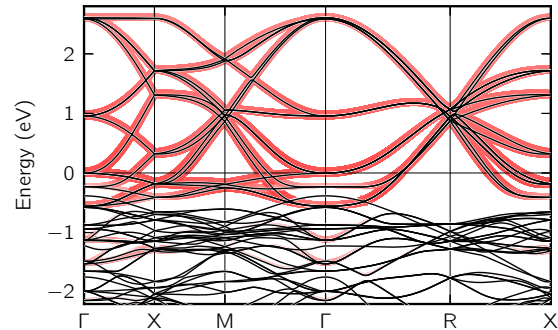

FIG. 5. (Color online) Bulk band structure of the $2 \times 2 \times 2$ supercell (black thin curves). Projections of the bands onto Wannier functions with Ni e_g character are indicated by red overlays where the thickness is proportional to the projection. The Fermi level is at 0 eV.
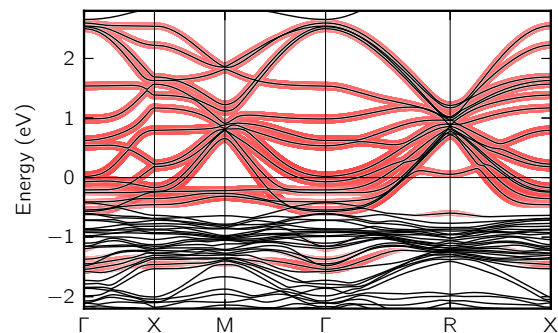

FIG. 6. (Color online) Band structure of a $2 \times 2 \times 2$ supercell with a single vacancy. Same nomenclature as Figure 5.

This type of discrepancy between formal electron counting and real-space based electron counting has been noted before: the change in electron count based on real-space counting is always significantly smaller, or at times essentially zero, when compared to formal charge values for many materials systems[53,54] Therefore, we continue our analysis in reciprocal space as well to understand the modification of band structure and band occupancy induced by the vacancy.

We compare the band structure of our $2\times2\times2$ LaNiO$_3$ supercell without and with the vacancy in Figures 5 and 6, respectively. The bulk band structure in Fig. 5 also shows projections onto the Ni Wannier functions of e_g symmetry: Ni^{3+} in bulk LaNiO$_3$ has 7 d electrons which fill the Ni d orbitals based on the crystal field splittings. The 3-fold degenerate lower energy t_{2g} manifold is full with 6 electrons and the 2-fold degenerate e_g manifold (composed of the $d_{3z^2-r^2}$ and $d_{x^2-y^2}$ orbitals) is quarter-filled with one electron. As expected from the crystal field analysis, the bands at the Fermi level are indeed of e_g character. We note that these e_g bands disperse over an energy range of ~3 eV.
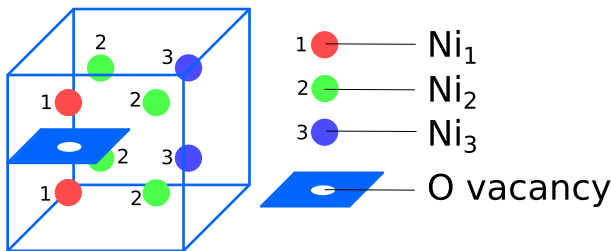
FIG. 7. (Color online) Classification of Ni atoms in a $2 \times 2 \times 2$ supercell based on the proximity to the oxygen vacancy. The vacancy is indicated by the white hole in the blue square, and the three types of inequivalent Ni site are indicated as well.

Figure 6 shows the band structure of a system with a single oxygen vacancy and projections onto the Ni e_g states. Compared to the bulk bands, the symmetry reduction has split some of the band energies across the Brillouin zone. We still have dispersive Ni e_g bands crossing the Fermi level. Critically, some weakly dispersing bands now appear about -1.5 eV below the Fermi level.

The next step is to examine local densities of states near and far from the vacancy. In a $2 \times 2 \times 2$ supercell, there are 8 distinct Ni sites which can be divided into three distinct groups depending on their proximity to the O vacancy as illustrated in Fig. 7. For a perfectly cubic perovskite structure, there are only three inequivalent Ni sites (see Fig. 7). In the fully relaxed rhombohedral structure with the vacancy, in principle more Ni sites become inequivalent. However, in order not to overcomplicate the analysis, we ignore the small symmetry breaking effects since we find that geometric proximity of Ni sites to the vacancy plays the dominant role.

Figure 8 shows projected density of states (PDOS) onto Ni $d_{3z^2-r^2}$, $d_{x^2-y^2}$, and t_{2g} Wannier functions for $2 \times 2 \times 2$ supercells with and without the vacancy. To align these densities of states along the energy axis, we have visually aligned the Ni PDOS of bulk LaNiO$_3$ to match as closely as possible that of Ni$_3$ in the system with the vacancy since Ni$_3$ is the farthest Ni from the vacancy site and thus should be most bulk like. (The qualitative nature of the alignment procedure is sufficient for our purpose of qualitative analysis of the PDOS.) We see that the PDOS of all Ni in the supercell closely resemble that of Ni in bulk LaNiO$_3$ with the exception of the $d_{3z^2-r^2}$ PDOS of Ni$_1$ adjacent to the vacancy. The Ni$_1$ $d_{3z^2-r^2}$ is narrowed compared to the bulk and its main peaks have moved to lower energies. The physical reasons for these modifications are straightforward and two-fold: these orbital point at the vacancy, and the removal of the oxygen O^{2-} ion (i) lowers their electrostatic crystal field energy, and (ii) the removal of the anti-bonding O p_z-Ni $d_{3z^2-r^2}$ interaction also lowers the energy of these orbitals (reduced covalency) and reduces their electronic connection to the lattice (reduced band width). In addition, we see the creation of a sharp peak in the Ni$_1$ $d_{3z^2-r^2}$ PDOS near -1.5 eV below the Fermi level which
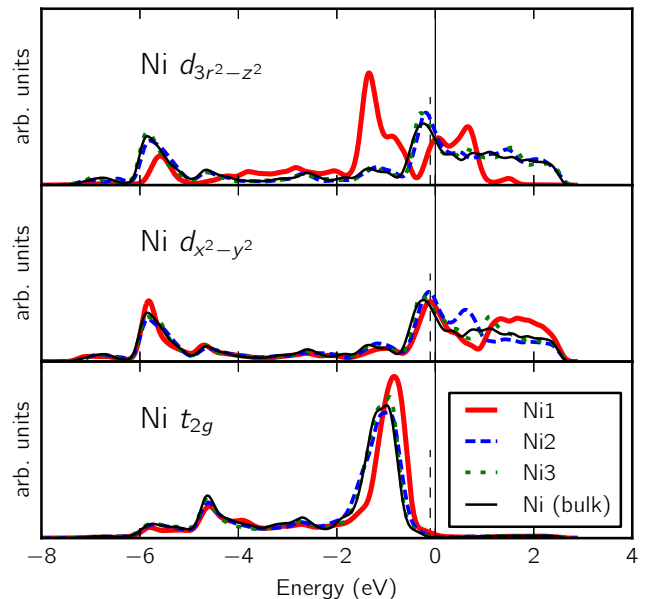

FIG. 8. (Color online) Projected density of states (PDOS) onto the Ni $3d$ Wannier functions for $2 \times 2 \times 2$ supercell. The naming of the Ni sites is shown in Fig. 7. The Fermi level is at 0 eV. We also show the Ni PDOS for bulk LaNiO$_3$ which is aligned in energy to match that of Ni$_3$ as closely as possible. The resulting position of the Fermi level of the bulk PDOS is indicated by the vertical dashed line.

is tied to the weakly dispersive bands observed in the band structure of Fig. 6. Furthermore, this ties in with the electron transfer to Ni observed in Fig. 4 where the lobes of the Ni orbitals accepting electrons resemble those of $d_{3z^2-r^2}$ states.

Up to now, our electronic structure calculations show that the creation of the neutral oxygen vacancy leads to significant electron transfer to localized states on the neighboring Ni sites into orbitals of primarily $d_{3z^2-r^2}$ character pointing at the vacancy site. To be able to make a more quantitative assessment and to decide on the exact degree of localized versus delocalized electron transfer form the vacancy, we need a more precise analysis.

We provide a simple and general analysis of the doping effect for a metallic system at zero temperature within band theory to organize our thinking. Let $d_0(E)$ be the density of states (DOS) per formula unit for bulk LaNiO$_3$ and $E_{F,0}$ the associated bulk Fermi level which corresponds to m electrons per formula unit. Let $D(E)$, E_F, and M be the corresponding quantities for a large supercell with $N \gg 1$ formula units containing one vacancy. The dilute nature of the vacancy means that $D(E)$ differs from $Nd_0(E)$ by a quantity of order $O(N^0) = O(1)$. Thus we can write $D(E) = Nd_0(E) + \Delta D(E)$ where the modification of the DOS, $\Delta D(E)$, is $O(1)$. The creation of the vacancy via removal of a neutral oxygen atom corresponds to a change in the number of electrons by δ for

the large supercell. In our case, $\delta = -4$, corresponding to the removal of four $2p$ electrons along with the neutral oxygen atom (we can ignore the deep lying $2s$ states in this analysis). Hence $M = Nm + \delta$. The Fermi levels are determined via

$$m = \int_{-\infty}^{E_{\mathrm{F},0}} dE\, d_0(E)$$

and

$$M = \int_{-\infty}^{E_{\mathrm{F}}} dE\, D(E)$$

which is equivalent to

$$Nm + \delta = \int_{-\infty}^{E_{\mathrm{F}}} dE\, [Nd_0(E) + \Delta D(E)] \,.$$

We also define the change of Fermi level $\Delta E_{\mathrm{F}} = E_{\mathrm{F}} - E_{\mathrm{F},0}$. The quantities δ and $\Delta D(E)$ scale as $O(N^0)$ while ΔE_{F} scales as $O(N^{-1})$. Therefore, we can expand the above relation to leading order in powers of N^{-1} to arrive at

$$\Delta E_{\mathrm{F}} = \frac{\delta - \int_{-\infty}^{E_{\mathrm{F},0}} dE\, \Delta D(E)}{N d_0(E_{\mathrm{F},0})} \quad (1)$$

This relation is useful in understanding what one can expect in the general case. The rigid band doping model corresponds to the case where $\Delta D(E)$ only stems from the removal of three O $2p$ bands from the valence band manifold of the supercell (since each O atom contributes three $2p$ states to valence band formation). In this case, the numerator of Eq. (1) is simply the number 2 — the integral in the numerator is -6 as three filled O $2p$ bands are removed upon creation of the vacancy — and we recover the rigid band doping relation for the Fermi level shift where $\Delta E_{\mathrm{F}} \propto 1/N$. The opposite limit is when a bound state for the vacancy appears below the Fermi energy which can accommodate all the doped electrons: in this case the numerator is zero and the Fermi level does not shift so no mobile electrons were added. Finally, one can always have an intermediate situation where the numerators is between the two extremes so we have partial doping: on average, a fraction of the two available electrons are mobile and the rest are bound around the vacancy. We note that the last situation can only happen for a metallic system where the Fermi level is crossing a finite density of states of some bands. In gapped systems, if a bound defect state is created in the energy gap, it binds all electrons and no mobile electrons are created; if no bound state forms, all the electrons are added or removed at the band edges which are always delocalized Bloch states and are mobile.

These general considerations explain that the change of Fermi level is the important quantity to monitor as it tells us whether far from the vacancy any mobile electrons are added in the bulk-like regions which corresponds to

TABLE III. Relation between the change of Fermi level ΔE_F, Ni $3d$ Löwdin occupations, and the number of added electrons per Ni atom in bulk LaNiO$_3$ within a rigid-band model. The second and fourth row correspond to two added electrons in the $4 \times 4 \times 4$ and $2 \times 2 \times 2$ supercells, respectively.

Doping (e/Ni)	ΔE_{F} (eV)	Ni $3d$ occupation (e)
0.000	0.000	8.374
0.031=2/64	0.017	8.393
0.125=2/16	0.070	8.449
0.250=2/8	0.153	8.523
0.375	0.258	8.595
0.500=2/4	0.375	8.665

doping in band theory. If $\Delta E_F \propto 1/N$ we have mobile electrons being doped; oppositely, a faster scaling to zero than $1/N$ indicates that bound states have formed below the Fermi level that accommodated all the electrons. To find ΔE_F, it is easier to monitor orbital occupancies — which are monotonic function of E_F — rather than the Fermi level itself. Namely, we monitor the number of $3d$ electrons on a Ni site far from the vacancy to understand the change of Fermi level.

The first step is to examine how adding electrons to bulk LaNiO$_3$ changes the Fermi level and Ni $3d$ occupations. We do this within a rigid-band model: we compute the electronic structure and densities of states of bulk LaNiO$_3$, and then add some electrons to these fixed bands and find the corresponding E_{F} and Ni $3d$ filling. Table III displays such data for bulk LaNiO$_3$: values of the Ni $3d$ electron count and corresponding Fermi level for a range of electron addition values. We now compare these values to those obtained from our supercell calculations that have vacancies.

For the $2 \times 2 \times 2$ supercell, the Ni $3d$ occupation for the Ni farthest from the vacancy (Ni$_3$), which is the most bulk like, is found to be 8.399. Separately, we integrate the bulk Ni PDOS and find that such a change corresponds to a rise of the Fermi level by 0.023 eV. This value is 6 time smaller than the value of 0.153 eV (fourth row of Table III) that we would expect for a rigid band model for doping by 2 electrons in a unit cell with 8 Ni cations. Next, we create a $4 \times 4 \times 4$ supercell atom supercell with 64 Ni cations and with a single oxygen vacancy and fully relaxed its structure (319 atom supercell). The $3d$ electron count on the Ni farthest from the vacancy is now 8.375 which corresponds to shifting the bulk Fermi level by 5×10^{-4} eV: this is 34 times smaller than the expected rigid band model shift of 0.017 eV from Table III. We conclude that the oxygen vacancy creates a bound state below the Fermi level that accommodates both electrons: the isolated vacancy is not an electron donor in the sense of donating mobile electrons. In other words, when we create an oxygen vacancy, the two neighboring Ni ions to the vacancy site each accept one electron on a highly localized state so that we have two Ni^{2+} ions surrounding the vacancy: the electron transfer is extremely localized and bound around the vacancy site.

C. Vacancy formation energy

The formation energy of a neutral oxygen vacancy is given by[55,56]

$$E_{V_O}^f(\mu_O) = E(V_O) - E(\text{bulk}) + \frac{1}{2}E(O_2) + \mu_O, \quad (2)$$

where μ_O is the chemical potential of oxygen atoms referenced to the half of the total energy of the O_2 molecule in its triplet ground state $E(O_2)$, $E(V_O)$ is the total energy of a supercell containing the vacancy, and $E(\text{bulk})$ is the total energy of a corresponding bulk supercell. The formation energy primarily depends on the imposed external conditions (temperature and pressure) through the chemical potential μ_O.

By definition, $\mu_O = 0$ corresponds to the oxygen-rich limit. In the opposite oxygen-poor limit, μ_O is limited from below by the decomposition of LaNiO$_3$ into other phases. Here, we estimate the lower bound based on the formation of La$_3$Ni$_3$O$_8$. The condition of equilibrium between LaNiO$_3$ and La$_3$Ni$_3$O$_8$ determines our minimum μ_O as

$$\mu_O^{min} = 3E(\text{LaNiO}_3) - E(\text{La}_3\text{Ni}_3\text{O}_8) - \frac{1}{2}E(O_2). \quad (3)$$

Both Eqs. (2) and (3) involve the total energy of the O_2 molecule in its ground state, which contains a substantial error within usual approximations for DFT.[57] In particular, the formation energies predicted by the above equations differ substantially when different pseudopotentials or different exchange-correlation approximations are used. For example, in Table IV, we compare results based on the LDA and PBE exchange-correlation functionals (columns marked LDA and PBE, respectively) using the $2 \times 2 \times 2$ supercell. We see that the vacancy formation energies in the oxygen-rich limit differ by a large amount of ~ 0.8 eV.

To correct this large error originating primarily from the error in $E(O_2)$, we use the approach of Finnis, Lozovoi, and Alavi (FLA).[58] Here, one does not explicitly compute the gas phase energy $E(O_2)$ but instead uses energies from the solid state and corrects the formation enthalpy to match experiment (one approximates theoretical enthalpies by energies). For example, by using the experimental formation enthalpy of Al$_2$O$_3$ from the reaction of bulk fcc Al and O_2 gas, $\Delta H^f(\text{Al}_2\text{O}_3)$, the corrected energy $E(O_2)$ is

$$\frac{1}{2}E(O_2) = \frac{1}{3}\left\{E(\text{Al}_2\text{O}_3) - 2E(\text{Al}) - \Delta H^f(\text{Al}_2\text{O}_3)\right\}. \quad (4)$$

Here, the total energies of bulk Al$_2$O$_3$, $E(\text{Al}_2\text{O}_3)$, and bulk fcc aluminum, $E(\text{Al})$, are calculated by DFT while the formation enthalpy $\Delta H^f(\text{Al}_2\text{O}_3) = -17.37$ eV is the experimental value.[59] Again, the advantage of this method is that it avoids theoretical computation of the gas phase $E(O_2)$ and relies only on solid state formation energies and enthalpies. The FLA-based formation

TABLE IV. Formation energy obtained using the $2 \times 2 \times 2$ supercell of LaNiO$_3$ calculated using LDA and PBE exchange-correlation functionals with and without the FLA correction.[58] The last row shows the lower bound on oxygen chemical potential computed with Eq. 3.
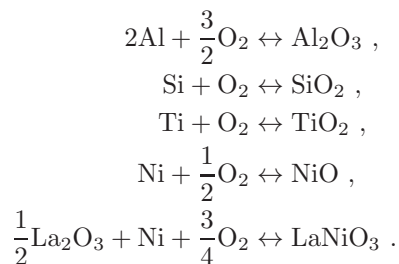
E^f (eV)	LDA	FLA-LDA	PBE	FLA-PBE
Oxygen-rich limit	3.00	2.92	2.24	2.97
Oxygen-poor limit	-0.10	-0.10	-0.35	-0.35
μ_O^{min} (eV)	-3.10	-3.02	-2.59	-3.32

energies using Eq. (4) are shown in Table IV as columns FLA-LDA and FLA-PBE. Happily, there is a much closer agreement between LDA and PBE in the oxygen-rich limit. The formation energy in the oxygen-poor limit does not actually depend on the value of $E(O_2)$ (combine Eqs. (2) and (3)) so that the corresponding entries in Table IV have the same values before and after the FLA correction.

A simple way to approximately gauge the accuracy of the FLA-based formation energies is to compare predictions from two different exchange-correlation approximations (LDA and PBE) for a fixed set of bulk materials energies — here those in Eq. (4). By comparing results for both oxygen-poor and oxygen-rich conditions, the error in the calculation seems to be ~ 0.2 eV. Of course, a larger set of exchange-correlation approximations should be used to test the robustness of this estimate, but such a tabulation is beyond the scope of this initial study.

A more challenging way to estimate the accuracy is to also use multiple bulk reference materials. We note that the use of Al$_2$O$_3$ simply follows the original FLA recipe, but any other bulk oxide reaction could be used as a reference to extract $E(O_2)$: our purpose in using the FLA is simply to remove the large error stemming from the poor description of the O_2 molecule. However, using a variety of reference bulk materials and then comparing the results implicitly assumes that the DFT calculation is equally accurate over the range of bulk materials, a potentially problematic assumption that requires care when dealing with transition metal oxides.

To illustrate this point, we calculate the FLA-based oxygen vacancy formation energy in the oxygen-rich limit based on five different reference oxide materials. The solid state reactions considered are

$$2\text{Al} + \frac{3}{2}O_2 \leftrightarrow \text{Al}_2\text{O}_3,$$
$$\text{Si} + O_2 \leftrightarrow \text{SiO}_2,$$
$$\text{Ti} + O_2 \leftrightarrow \text{TiO}_2,$$
$$\text{Ni} + \frac{1}{2}O_2 \leftrightarrow \text{NiO},$$
$$\frac{1}{2}\text{La}_2\text{O}_3 + \text{Ni} + \frac{3}{4}O_2 \leftrightarrow \text{LaNiO}_3.$$

The resulting FLA-LDA and FLA-PBE formation energies are presented in Table V. As the table shows, almost all values of the vacancy formation energy agree

TABLE V. Oxygen vacancy formation energy in eV per vacancy obtained using the $2 \times 2 \times 2$ supercell of $LaNiO_3$. Both LDA and GGA exchange-correlation functionals are employed together with the FLA correction[58] based on the listed reference oxides. The experimental formation enthalpies in eV from the literature are provided as well. The averages and variances do not include the NiO data (see text for why).

Reference	FLA-LDA	FLA-PBE	Formation enthalpy
Al_2O_3	2.92	2.97	-17.37[a]
SiO_2	3.03	2.95	-9.44[a]
TiO_2	2.65	2.70	-9.73[a]
NiO	3.93	3.80	-2.49[b]
$LaNiO_3$	2.81	2.62	-3.08[c]
Average	2.85	2.81	
Sample variance	0.16	0.18	

[a] Ref. 59
[b] Ref. 61
[c] Ref. 62

well with each other with the exception of those based on the NiO reference. Prior work has shown that in addition to the error in $E(O_2)$ discussed above, DFT-based formation energies for transition-metal oxides also can suffer from significant errors due to the an inadequate description of strong electron correlation effects.[60] In particular, NiO and MnO were shown to be the most affected, and the DFT+U approach can be used to overcome the deficiency.[60] In our case, this type of correction is problematic since it is non-trivial to describe NiO and $LaNiO_3$ equally well for a fixed exchange-correlation approximation: as per Section II, $LaNiO_3$ is best described by LDA whereas NiO has a poor LDA formation energy. For this reason, we view NiO as a systematic outlier and exclude it as a reference material (this is also the reason we chose the formation reaction for $LaNiO_3$ to involve fcc metallic Ni and not NiO). Separately, while TiO_2 is also a $3d$ transition-metal oxide, it suffers less from the strong-electron-correlation problem[60] leading to more reasonable results for oxygen vacancy formation energy in Table V. Based on the data in the table not involving NiO, we estimate the accuracy of the formation energy with the FLA method to be about ~ 0.2 eV.

The next step involves the removal of finite size errors and extrapolation to the thermodynamic limit of an isolated vacancy. To this end, we have computed the vacancy formation energy in the oxygen rich limit using a number of additional supercell with sizes ranging from 4 to 319 atoms. For the four smallest supercells, we have also computed PBE-based formation energies. The results of these calculations are shown in Fig. 9, where formation energies are plotted versus the inverse characteristic size of the supercell, $L^{-1} = V^{-1/3}$, where V is the supercell volume.

Fig. 9 shows good agreement between LDA and PBE for all supercells. We extrapolate to infinite-sized super-
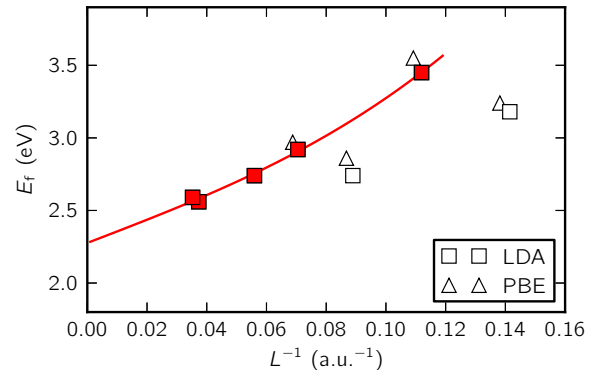

FIG. 9. (Color online) Formation energies calculated using supercells of various sizes in the oxygen-rich limit with LDA and PBE exchange-correlation functionals. The extrapolation to infinite cell size is made using similar supercells within LDA (filled squares) and is shown with a solid line.

cell using the form[63]

$$E^{f}(L) = E^{f}_{\infty} + a_1 L^{-1} + a_3 L^{-3} \quad (5)$$

where E^{f}_{∞} is the desired formation energy in the infinite supercell limit. To perform the extrapolation, we only use supercells that describe the structure of bulk $LaNiO_3$ properly. For example, the 4 atom unit cell originates from a 5 atom cubic perovskite unit cell of $LaNiO_3$ which can not describe the oxygen octahedral rotations present in bulk $LaNiO_3$. Specifically, we consider $2 \times 2 \times 2$ (40 atoms) and $4 \times 4 \times 4$ (320 atoms) pseudocubic supercells, as well as $1 \times 1 \times 1$ (10 atoms), $2 \times 2 \times 2$ (80 atoms) and $3 \times 3 \times 3$ (270 atoms) rhombohedral supercells. These supercells are indicated by the filled squares in Fig. 9.

By performing a least squares fit of our data to Eq. (5), we find $E^{f}_{\infty} = 2.28$ eV in the oxygen-rich limit and -0.82 eV in the oxygen poor limit. This result means the formation of oxygen vacancies becomes *thermodynamically* favored when the chemical potential of oxygen μ_O becomes less than ≈ -2.3 eV. To translate this into experimental conditions, by using the relation

$$\mu_O(T, p_{O_2}) = \frac{1}{2} g_{O_2}(T) + \frac{1}{2} k_B T \ln \left\{ \frac{p_{O_2}}{1 \text{ atm}} \right\}, \quad (6)$$

where values of $g_{O_2}(T)$ are taken from experiment,[64] we find that for a partial pressure of oxygen of 10^{-7} torr, $\mu_O = -2.3$ eV corresponds to a temperature of 1000 K. Another useful comparison is to $SrTiO_3$ where the theoretically computed formation energy is much larger at ~ 6 eV in the oxygen rich limit.[65] Despite this large value, it is well known that oxygen vacancies can be formed in $SrTiO_3$ easily in vacuum at high temperatures. Compared to $SrTiO_3$, $LaNiO_3$ has a much stronger preference for oxygen vacancy formation.

TABLE VI. Energy barrier, E_b, computed using NEB as a function of number of atoms.

# of atoms	4	9	39	79
E_b (eV)	1.16	1.27	1.37	1.24

D. Energy barrier for vacancy propagation

The mobility of oxygen vacancies plays an important role in the annealing, oxidation, and reduction of metal oxides. To get an idea of the mobility of oxygen vacancies in $LaNiO_3$, we performed nudged-elastic-band (NEB)[66] calculations for a vacancy propagating from one site to the nearest equivalent site. In bulk $LaNiO_3$ (Section III A, all O sites are related by symmetry so there is a single energy barrier to be computed. The NEB calculation determines the most favorable reaction path for vacancy propagation and the energy profile along the path. The energy barrier height along the path is a measure of the defect mobility.

Unlike calculation of the formation energy described in a previous section, the NEB requires a series of total-energy calculations with a *fixed* number of atoms, and therefore we expect the LDA to be sufficient for this computation. Table VI shows the calculated barrier height E_b using several supercells. One can see that E_b changes little with increasing supercell size. The 4-atom cell NEB calculation is based on a 5-atom parent unit cell of bulk $LaNiO_3$ that corresponds to an ideal cubic perovskite structure which has higher symmetry than the actual ground state of $LaNiO_3$. However, one can see that this calculation already provides a good estimate for the NEB energy barrier height.

Our best estimate for the barrier height obtained with the 79-atom supercell is 1.24 eV. We can compare this result to the corresponding barrier height of 0.6 eV for oxygen vacancy in $SrTiO_3$.[67] Thus, we conclude that oxygen vacancies in $LaNiO_3$ might be happier to form from the energetic viewpoint but are much less mobile than oxygen vacancies in $SrTiO_3$. Transition state theory allows us to quantify this difference: at room temperature, a vacancy diffuses to a neighboring site in ~ 1 ms in $SrTiO_3$ while it takes ~ 2 years for it to happen in $LaNiO_3$.

E. Vacancy interactions

To understand the segregation tendencies of oxygen vacancies in $LaNiO_3$, we performed total-energy calculations using $2 \times 2 \times 2$ supercells containing two oxygen vacancies. If we ignore the effects of distortion of the lattice away from the ideal perovskite structure, there are 7 distinct ways to arrange two oxygen vacancies in a $2 \times 2 \times 2$ supercell. These are shown schematically in Fig. 10. We performed structural relaxations on these 7 systems keeping the supercell shape and volume fixed.

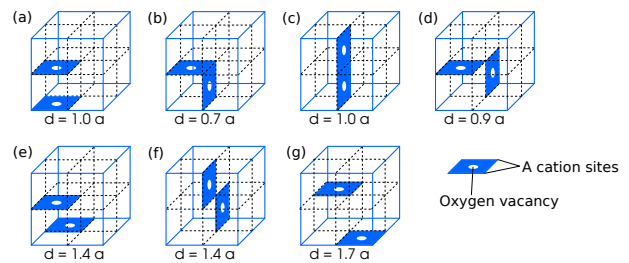The formation energy of a pair of oxygen vacancies

FIG. 10. (Color online) Schematic illustration of the 7 distinct configurations for two oxygen vacancies in a $2 \times 2 \times 2$ $LaNiO_3$ supercell. The solid blue lines indicate the volume of the supercell. Dashed black lines indicate the 8 interior pseudo-cubic $1 \times 1 \times 1$ cells (each has one formula unit). The positions of the two vacancies are indicated by the blue squares. As the legend in the lower right shows, the vacancy position is at the center of a square (the white hole) and A site cations (La) are on the corners of the square. The orientation of the square shows the plane bisecting the line between the two Ni neighboring a vacancy. The *approximate* distance between two vacancies for each case is indicated in units of the $1 \times 1 \times 1$ pseudocubic lattice constant a.

TABLE VII. Divacancy binding energies computed using Eq. (8) in a $2 \times 2 \times 2$ supercell. The configurations are those shown in Fig. 10. The (shortest) relaxed distance between the vacancy pair for each configuration is given in units of the pseudocubic lattice constant a.

Divacancy configuration	(a)	(b)	(c)	(d)	(e)	(f)	(g)
Vacancy separation (a)	1.0	0.7	1.0	0.9	1.4	1.4	1.7
$E_{2V_O}^{bind}$ (eV)	−0.38	0.38	0.13	0.23	0.40	0.37	0.15

(divacancy) is given by

$$E_{2V_O}^f(\mu_O) = E(2V_O) - E(\text{bulk}) + E(O_2) + 2\mu_O. \quad (7)$$

However, it is more informative to consider the binding energy of the divacancy given by

$$E_{2V_O}^{bind} = E_{2V_O}^f - 2E_{V_O}^f = E(2V_O) - 2E(V_O) + E(\text{bulk}). \quad (8)$$

This is the energy of the divacancy relative to a pair of vacancies at infinite separation. This binding energy does not depend on the chemical potential. A negative binding energies mean the divacancy configuration is more favorable than separated vacancies.

The binding energies are presented in Table VII. Divacancy configuration (a) from Fig. 10 is the only stable case. Therefore, vacancies generally repel each other so there is an energy barrier for them to cross before forming the stable bound structure (a).

In configuration (a), the vacancies line up along a pseudocubic axis and are on opposite sides of one Ni atom. A similar observation was made by Cuong *et al.*[67] in their study of oxygen vacancies in perovskite $SrTiO_3$. These authors referred to such a configuration of a pair of vacancies as an *apical divacancy*. They calculated the band structure of $SrTiO_3$ with an apical divacancy and found
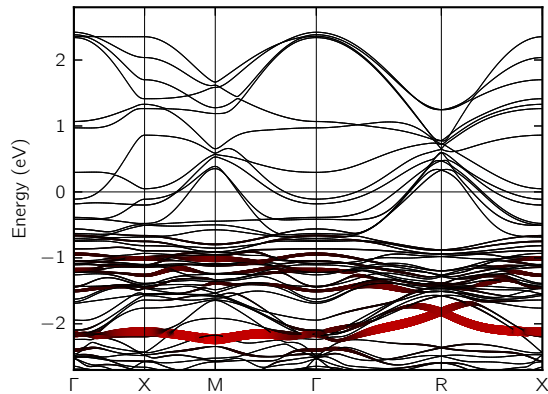
FIG. 11. (Color online) Band structure of a $2 \times 2 \times 2$ supercell with an apical divacancy, projected on the $d_{3z^2-r^2}$ Wannier functions of the Ni atoms nearest to vacancies.

FIG. 12. (Color online) c/a as a function of O vacancy concentration in tetragonal $LaNiO_{3-\delta}$.

that a low-energy flat defect band (localized state) forms in the bulk band gap. The stability of the divacancy is then attributed to the low-energy nature of the defect state: electrons prefer to fill these states instead of those of the isolated vacancy.

Figure 11 shows our computed band structure for the stable divacancy configuration in $LaNiO_3$. Although in the case of $LaNiO_3$ there is no band gap, we see that a nearly flat band forms below the Fermi level. Thus, by analogy with $SrTiO_3$, we can conclude that the apical divacancy creates favorable low-energy localized states for electrons to fill thereby rationalizing the stability of the divacancy configuration.

F. Oxygen reduced lanthanum-nickelate phases

When the number of vacancies increases and reaches finite concentrations, phases of lanthanum nickel oxide other than the perovskite formula ($LaNiO_3$) are stabilized.[68,69] In this section, we examine a number of such $LaNiO_{3-\delta}$ structures where the oxygen deficiency $0 \leq \delta \leq 1$, and for simplicity, focus primarily on the effect of the oxygen vacancies on the lattice parameters of the materials. The primary reason is that such results are useful for experimental determination of approximate oxygen content of a new material or thin film since measurements of lattice parameters are straightforward using x-ray methods. While it is well know that the density of defects in oxides modifies their lattice parameters, the lack of reliable data on a wide range of oxygen content makes this structure-property relationship in $LaNiO_{3-\delta}$ structures a subject where first principles theory can provide useful guidance.

In our analysis, we limit ourselves to those materials which are derived from perovskite $LaNiO_3$ by lining up the oxygen vacancies along the pseudocubic axes. This decision is based on our results from the previous section,
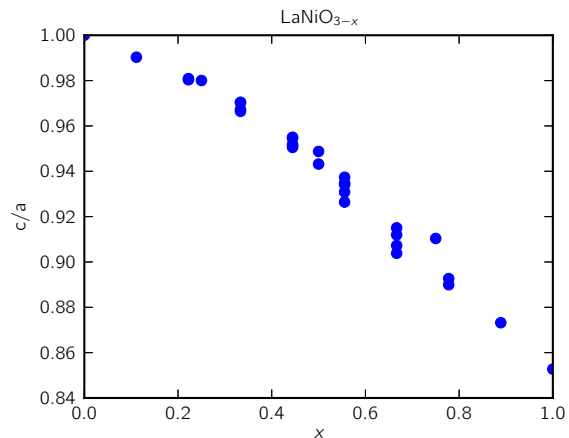
showing that divacancies are most stable when aligned along a pseudocubic axis, and due to experimental evidence on actual materials.[68,69] In addition, to simplify the calculations and ease the comparison of various structures, we enforce tetragonal symmetry of the Bravais lattice in our calculations so that the in-plane lattice were equal ($a = b$). While this is a theoretical restriction for bulk phases of $LaNiO_{3-\delta}$, pragmatically the use of tetragonal symmetry is justified by the fact that thin films of $LaNiO_3$ are typically grown on the substrates with square in-plane symmetry, such as (001) $LaAlO_3$ and $SrTiO_3$. The epitaxial constraint then forces a tetragonal structure on the thin film. For what follows, we used $n \times n \times 1$ supercells, considered $n \leq 3$, and relaxed all atomic positions and the two lattice parameters a and c.

Figures 12 and 13 show the dependence of the c/a ratio and unit cell volume on the oxygen vacancy concentration δ. One can see that c/a ratio decreases monotonically by about 15% as δ changes from 0 to 1. The volume, on the other hand, remains almost constant for δ up to ~ 0.4 and then decreases. The comparison to available experimental data is fair especially given the wide spread in nominally identical experimental systems at $\delta = 0.5$. Smaller scale discrepancies are also likely due to the fact that we enforced orthogonality for $La_2Ni_2O_5$ systems (with in-plane lattice constants $a = b$) whereas experimentally they were found to be monoclinic.[68]

For the case of $LaNiO_3$ thin films, we calculated the dependence of the relaxed out-of-plane parameter c/a for $LaNiO_{3-\delta}$ systems strained to $LaAlO_3$ substrate (see Fig. 14). We find that in this case the c/a ratio decreases less rapidly that for the bulk cases as it becomes $\sim 10\%$ smaller as δ goes to 1. This data can be used to calibrate the oxygen content of $LaNiO_3$ thin films based on their c/a parameters.
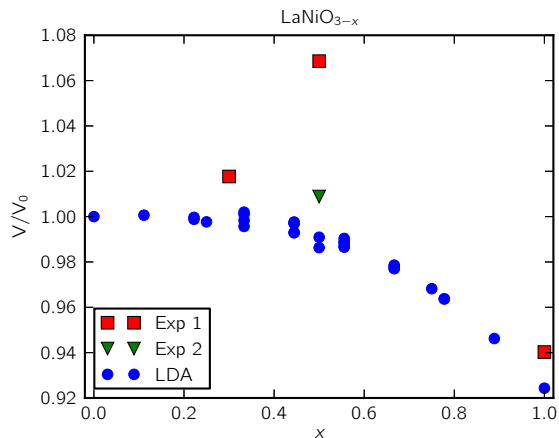
FIG. 13. (Color online) V/V_0 as a function of O vacancy concentration in tetragonal $LaNiO_{3-\delta}$. The labels 'Exp 1' and 'Exp 2' denote results from Refs. 68 and 69, respectively.
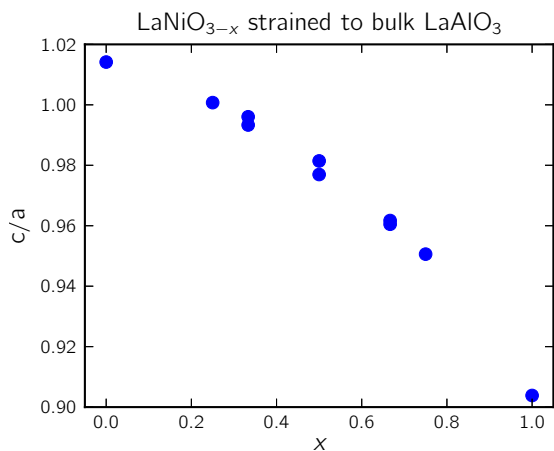

FIG. 14. (Color online) c/a as a function of O vacancy concentration in tetragonal $LaNiO_{3-\delta}$. The in-plane lattice parameters are strained to those of bulk $LaAlO_3$.

IV. SUMMARY

We performed first-principles study of properties of oxygen vacancies in $LaNiO_3$. Our analysis of the electronic structure of $LaNiO_3$ with an isolated neutral oxygen vacancy shows that introduction of this defect results in the formation of a localized states with the energy ~ 1.5 eV below the Fermi level. These states accept the two electrons that are released upon removal of a neutral atom from the material. Thus, an oxygen vacancy does not act as a donor in the sense of adding mobile carriers at the Fermi level; instead, each vacancy donates an electron to localized states on the two Ni ions neighboring the vacancy and thus creates two Ni^{2+} ions. If we choose the oxygen vacancy to occur between to Ni separated by a pseudocubic lattice constant along the z direction, then the localized states accepting electrons are essentially the $d_{3z^2-r^2}$ orbitals of the two Ni ions adjacent to the vacancy. The $d_{3z^2-r^2}$ orbitals on these two Ni ions form narrower bands and are at lower energies when compared to bulk-like Ni ions that are fully oxygen coordinated. Many of these electronic state modifications are in agreement with previous studies of surfaces of (001) NiO_2-terminated $LaNiO_3$ films where the surface Ni atoms have missing oxygen neighbors and thus have very similar densities of states for the Ni $d_{3z^2-r^2}$ orbitals.[18,25,30]

We also calculated the basic thermodynamic and kinetic properties of oxygen vacancy such as the vacancy formation energy and energy barrier for vacancy propagation. We find that formation of oxygen vacancies in $LaNiO_3$ becomes thermodynamically favorable for oxygen chemical potential μ_O below -2.3 eV. The energy barrier for oxygen vacancy diffusion was found to be 1.24 eV. These results allow us to make a comparison to $SrTiO_3$ and conclude that oxygen vacancies are easier to form in $LaNiO_3$ compared to $SrTiO_3$ but are much less mobile.

Finally, we analyzed the segregation tendencies of oxygen vacancies by looking at the energetics of a pair of oxygen vacancies. Oxygen vacancies are found to prefer to form lines along pseudocubic axes. For finite concentrations of oxygen vacancies, we described the dependence of lattice parameters on vacancy concentration. Our results may be useful for experimentalists as a straightforward approach to determine the oxygen vacancy concentration based on the lattice parameters measurements.

* andrei.malashevich@yale.edu

[1] M. L. Medarde, J. Phys.: Condens. Matter **9**, 1679 (1997).

[2] G. Catalan, Phase Transit. **81**, 729 (2008).

[3] P. Zubko, S. Gariglio, M. Gabay, P. Ghosez, and J.-M. Triscone, Annu. Rev. Condens. Matter Phys. **2**, 141 (2011).

[4] J. B. Torrance, P. Lacorre, A. I. Nazzal, E. J. Ansaldo, and C. Niedermayer, Phys. Rev. B **45**, 8209 (1992).

[5] J. L. García-Muñoz, J. Rodríguez-Carvajal, P. Lacorre, and J. B. Torrance, Phys. Rev. B **46**, 4414 (1992).

[6] J. A. Alonso, J. L. García-Muñoz, M. T. Fernández-Díaz, M. A. G. Aranda, M. J. Martínez-Lope, and M. T. Casais,

Phys. Rev. Lett. **82**, 3871 (1999).

[7] J. A. Alonso, M. J. Martínez-Lope, M. T. Casais, J. L. García-Muñoz, and M. T. Fernández-Díaz, Phys. Rev. B **61**, 1756 (2000).

[8] M. Zaghrioui, A. Bulou, P. Lacorre, and P. Laffez, Phys. Rev. B **64**, 081102 (2001).

[9] U. Staub, G. I. Meijer, F. Fauth, R. Allenspach, J. G. Bednorz, J. Karpinski, S. M. Kazakov, L. Paolasini, and F. d'Acapito, Phys. Rev. Lett. **107**, 206804 (2011).

[10] M. Gibert, P. Zubko, R. Scherwitzl, J. Íñiguez, and J.-M. Triscone, Nat. Mater. **11**, 195 (2012).

[11] H. Ichinose, M. Nagano, H. Katsuki, and H. Takagi, J. Mater. Sci. **29**, 5115 (1994).

[12] C.-C. Yang, M.-S. Chen, T.-J. Hong, C.-M. Wu, J.-M. Wu, and T.-B. Wu, Appl. Phys. Lett. **66**, 2643 (1995).

[13] P. Murugavel, R. Sharma, A. R. Raju, and C. N. R. Rao, J. Phys. D: Appl. Phys. **33**, 906 (2000).

[14] M. Jain, B. S. Kang, and Q. X. Jia, Appl. Phys. Lett. **89**, 242903 (2006).

[15] K.-T. Kim, C.-I. Kim, J.-G. Kim, and G.-H. Kim, Thin Solid Films **515**, 8082 (2007).

[16] J. Son, P. Moetakef, J. M. LeBeau, D. Ouellette, L. Balents, S. J. Allen, and S. Stemmer, Appl. Phys. Lett. **96**, 062114 (2010).

[17] R. Scherwitzl, S. Gariglio, M. Gabay, P. Zubko, M. Gibert, and J.-M. Triscone, Phys. Rev. Lett. **106**, 246403 (2011).

[18] D. P. Kumah, A. S. Disa, J. H. Ngai, H. Chen, A. Malashevich, J. W. Reiner, S. Ismail-Beigi, F. J. Walker, and C. H. Ahn, Advanced Materials **26**, 1935 (2014).

[19] J. Chaloupka and G. Khaliullin, Phys. Rev. Lett. **100**, 016404 (2008).

[20] S. J. May, T. S. Santos, and A. Bhattacharya, Phys. Rev. B **79**, 115127 (2009).

[21] P. Hansmann, X. Yang, A. Toschi, G. Khaliullin, O. K. Andersen, and K. Held, Phys. Rev. Lett. **103**, 016401 (2009).

[22] M. J. Han, C. A. Marianetti, and A. J. Millis, Phys. Rev. B **82**, 134408 (2010).

[23] J. Chakhalian, J. M. Rondinelli, J. Liu, B. A. Gray, M. Kareev, E. J. Moon, N. Prasai, J. L. Cohn, M. Varela, I. C. Tung, M. J. Bedzyk, S. G. Altendorf, F. Strigari, B. Dabrowski, L. H. Tjeng, P. J. Ryan, and J. W. Freeland, Phys. Rev. Lett. **107**, 116805 (2011).

[24] E. Benckiser, M. W. Haverkort, S. Brück, E. Goering, S. Macke, A. Frañó, X. Yang, O. K. Andersen, G. Cristiani, H.-U. Habermeier, A. V. Boris, I. Zegkinoglou, P. Wochner, H.-J. Kim, V. Hinkov, and B. Keimer, Nat. Mater. **10**, 189 (2011).

[25] M. J. Han, X. Wang, C. A. Marianetti, and A. J. Millis, Phys. Rev. Lett. **107**, 206804 (2011).

[26] M. J. Han and M. van Veenendaal, Phys. Rev. B **84**, 125137 (2011).

[27] J. W. Freeland, J. Liu, M. Kareev, B. Gray, J. W. Kim, P. Ryan, R. Pentcheva, and J. Chakhalian, Europhys. Lett. **96**, 57004 (2011).

[28] A. Blanca-Romero and R. Pentcheva, Phys. Rev. B **84**, 195450 (2011).

[29] A. V. Boris, Y. Matiks, E. Benckiser, A. Frano, P. Popovich, V. Hinkov, P. Wochner, M. Castro-Colin, E. Detemple, V. K. Malik, C. Bernhard, T. Prokscha, A. Suter, Z. Salman, E. Morenzoni, G. Cristiani, H.-U. Habermeier, and B. Keimer, Science **332**, 937 (2011).

[30] H. Chen, D. P. Kumah, A. S. Disa, F. J. Walker, C. H. Ahn, and S. Ismail-Beigi, Phys. Rev. Lett. **110**, 186402 (2013).

[31] A. S. Disa, D. P. Kumah, A. Malashevich, H. Chen, D. A. Arena, E. D. Specht, S. Ismail-Beigi, F. J. Walker, and C. H. Ahn, Phys. Rev. Lett. **114**, 026801 (2015).

[32] R. D. Sánchez, M. T. Causa, A. Caneiro, A. Butera, M. Vallet-Regí, M. J. Sayagués, J. González-Calbet, F. García-Sanz, and J. Rivas, Phys. Rev. B **54**, 16574 (1996).

[33] N. Gayathri, A. K. Raychaudhuri, X. Q. Xu, J. L. Peng, and R. L. Greene, J. Phys.: Condens. Matter **10**, 1323 (1998).

[34] A. Tiwari and K. P. Rajeev, J. Phys.: Condens. Matter **11**, 3291 (1999).

[35] M. Abbate, G. Zampieri, F. Prado, A. Caneiro, J. M. Gonzalez-Calbet, and M. Vallet-Regi, Phys. Rev. B **65**, 155101 (2002).

[36] M. T. Escote, F. M. Pontes, E. R. Leite, J. A. Varela, R. F. Jardim, and E. Longo, Thin Solid Films **445**, 54 (2003).

[37] J. Zaanen, G. A. Sawatzky, and J. W. Allen, Phys. Rev. Lett. **55**, 418 (1985).

[38] K. Horiba, R. Eguchi, M. Taguchi, A. Chainani, A. Kikkawa, Y. Senba, H. Ohashi, and S. Shin, Phys. Rev. B **76**, 155104 (2007).

[39] L. Qiao and X. Bi, Europhys. Lett. **93**, 57002 (2011).

[40] G. Gou, I. Grinberg, A. M. Rappe, and J. M. Rondinelli, Phys. Rev. B **84**, 144101 (2011).

[41] M. Jain, J. R. Chelikowsky, and S. G. Louie, Phys. Rev. Lett. **107**, 216803 (2011).

[42] A. Malashevich, M. Jain, and S. G. Louie, Phys. Rev. B **89**, 075205 (2014).

[43] P. Giannozzi, S. Baroni, N. Bonini, M. Calandra, R. Car, C. Cavazzoni, D. Ceresoli, G. L. Chiarotti, M. Cococcioni, I. Dabo, A. Dal Corso, S. de Gironcoli, S. Fabris, G. Fratesi, R. Gebauer, U. Gerstmann, C. Gougoussis, A. Kokalj, M. Lazzeri, L. Martin-Samos, N. Marzari, F. Mauri, R. Mazzarello, S. Paolini, A. Pasquarello, L. Paulatto, C. Sbraccia, S. Scandolo, G. Sclauzero, A. P. Seitsonen, A. Smogunov, P. Umari, and R. M. Wentzcovitch, J. Phys.: Condens. Matter **21**, 395502 (19pp) (2009).

[44] J. P. Perdew and A. Zunger, Phys. Rev. B **23**, 5048 (1981).

[45] J. P. Perdew, K. Burke, and M. Ernzerhof, Phys. Rev. Lett. **77**, 3865 (1996).

[46] D. Vanderbilt, Phys. Rev. B **41**, 7892 (1990).

[47] K. Laasonen, R. Car, C. Lee, and D. Vanderbilt, Phys. Rev. B **43**, 6796 (1991).

[48] S. G. Louie, S. Froyen, and M. L. Cohen, Phys. Rev. B **26**, 1738 (1982).

[49] N. Marzari and D. Vanderbilt, Phys. Rev. B **56**, 12847 (1997).

[50] I. Souza, N. Marzari, and D. Vanderbilt, Phys. Rev. B **65**, 035109 (2001).

[51] A. A. Mostofi, J. R. Yates, Y.-S. Lee, I. Souza, D. Vanderbilt, and N. Marzari, Computer Physics Communications **178**, 685 (2008).

[52] A. Y. Dobin, K. R. Nikolaev, I. N. Krivorotov, R. M. Wentzcovitch, E. D. Dahlberg, and A. M. Goldman, Phys. Rev. B **68**, 113408 (2003).

[53] W. Luo, A. Franceschetti, M. Varela, J. Tao, S. J. Pennycook, and S. T. Pantelides, Phys. Rev. Lett. **99**, 036402 (2007).

[54] H. Raebiger, S. Lany, and A. Zunger, Nature (London) **453**, 763 (2008).

[55] S. B. Zhang and J. E. Northrup, Phys. Rev. Lett. **67**, 2339 (1991).

[56] C. G. Van de Walle, D. B. Laks, G. F. Neumark, and S. T. Pantelides, Phys. Rev. B **47**, 9425 (1993).

[57] N. D. M. Hine, K. Frensch, W. M. C. Foulkes, and M. W. Finnis, Phys. Rev. B **79**, 024112 (2009).

[58] M. W. Finnis, A. Y. Lozovoi, and A. Alavi, Annu. Rev. Mater. Res. **35**, 167 (2005).

[59] M. W. Chase, Jr., J. Phys. Chem. Ref. Data, Monograph 9 , 1 (1998), http://webbook.nist.gov.

[60] L. Wang, T. Maxisch, and G. Ceder, Phys. Rev. B **73**, 195107 (2006).

[61] B. J. Boyle, E. G. King, and K. C. Conway, Journal of the American Chemical Society **76**, 3835 (1954).

[62] J. Cheng, A. Navrotsky, X.-D. Zhou, and H. U. Anderson, Journal of Materials Research **20**, 191 (2005).

[63] C. W. M. Castleton and S. Mirbt, Phys. Rev. B **70**, 195202 (2004).

[64] Http://webbook.nist.gov.

[65] J. P. Buban, H. Iddir, and S. Öğüt, Phys. Rev. B **69**, 180102 (2004).

[66] G. Henkelman, B. P. Uberuaga, and H. Jónsson, J. Chem. Phys. **113**, 9901 (2000).

[67] D. D. Cuong, B. Lee, K. M. Choi, H.-S. Ahn, S. Han, and J. Lee, Phys. Rev. Lett. **98**, 115503 (2007).

[68] M. Crespin, P. Levitz, and L. Gatineau, J. Chem. Soc., Faraday Trans. 2 **79**, 1181 (1983).

[69] T. Moriga, O. Usaka, I. Nakabayashi, T. Kinouchi, S. Kikkawa, and F. Kanamaru, Solid State Ionics **79**, 252 (1995).